Csp^3–H Bond Activation Mediated by a Pd(II) Complex under Mild Conditions

Hanah Na,[a,b,#] Andrew J. Wessel,[c,#] Seoung-Tae Kim,[d,e,#] Mu-Hyun Baik,[d,e,*] and Liviu M. Mirica[a,*]

[a] Department of Chemistry, University of Illinois at Urbana-Champaign, 600 S. Mathews Avenue, Urbana, Illinois, 61801

[b] Current address: Center for Advanced Specialty Chemicals, Korea Research Institute of Chemical Technology (KRICT), Ulsan 44412, Republic of Korea

[c] Department of Chemistry, Washington University, St. Louis, Missouri, 63130-4899

[d] Department of Chemistry, Korea Advanced Institute of Science and Technology (KAIST), Daejeon 34141, Republic of Korea

[e] Center for Catalytic Hydrocarbon Functionalizations, Institute for Basic Science (IBS), Daejeon 34141, Republic of Korea

[#] These authors contributed equally.

[*] Email: mbaik2805@kaist.ac.kr

[*] Email: mirica@illinois.edu

Abstract

In this work, we disclose a new pentadentate pyridinophane ligand, *N*-methyl-N'-(2-methylpyryl)-2,11-diaza[3.3](2,6)pyridinophane (^{PicCH3}N4), and its Pd(II) complexes. The reaction of the Pd precursor $[Pd^{II}(MeCN)_4]^{2+}$ with ^{PicCH3}N4 leads to the formation of the palladacycle compound $[(^{PicCH2}N4)Pd^{II}]^{+}$ via an uncommon room-temperature Csp^3–H bond activation at a Pd(II) metal center. The isolated complex was characterized by single-crystal X-ray diffraction, NMR spectroscopy, and cyclic voltammetry. Furthermore, various experimental investigations, including additive studies, kinetic isotope effect measurements, and Eyring analysis were carried out to probe the reaction kinetics and mechanism of the Csp^3–

H bond activation by the Pd(II) center. A combined experimental and theoretical mechanistic analysis suggests that acetate-assisted Csp^3–H bond activation is preferred at high temperature, while acetate-free Csp^3–H bond activation is preferred at room temperature.

Introduction

The coordination chemistry of metal complexes supported by macrocyclic ligands has experienced great growth during the past several decades, as macrocyclic ligands can serve as models for biologically important species or impart thermodynamic and kinetic stability to their metal complexes in unusual oxidation states that are otherwise uncommon or metastable with the noncyclic ligand congeners.[1-7] Although a significant number of macrocyclic coordinating ligands for metal ions have been reported, developing new types of macrocyclic ligands is still an attractive goal for further applications and studies in the field of coordination chemistry. Among various macrocycles, the tetradentate *N*,*N*′-dialkyl-2,11-diaza[3.3](2,6)pyridinophane (^{R}N4, R = ^{t}Bu, ^{i}Pr, Me) ligands can serve as robust igands for various metal ions (e. g., Pd, Ni, Cu, Co, Fe, Mn, Zn) and have been extensively investigated.[8-20] These tetradentate ^{R}N4 ligands provide unique environments to the coordinated metal center and enable various reactivity pathways for C–C/C–X bond formation,[11-12, 14, 16, 19-20] small molecule activation,[21-23] or water oxidation.[24-25] In contrast to tetradentate pyridinophane ligands, the reports on multidentate pyridinophane ligands with five or more donor atoms are sparse.[26-30] In order to explore new ligand scaffolds and investigate the related coordination chemistry, we report herein the synthesis of a new pentadentate pyridinophane ligand, *N*-methyl-N'-(2-methylpyryl)-2,11-diaza[3.3](2,6)pyridinophane (^{PicCH3}N4) and its Pd^{II} complexes. Interestingly, when the Pd^{II} precursor $[Pd^{II}(MeCN)_4]^{2+}$ was reacted with the ^{PicCH3}N4 ligand, the palladacycle compound $[(^{PicCH2}N4)Pd^{II}]^{+}$ was obtained, which formed via an uncommpn Csp^3–H activation of the ^{PicCH3}N4 ligand, under mild conditions and in absence

of any base additive. The isolated complex was characterized by single-crystal X-ray diffraction, NMR spectroscopy, and cyclic voltammetry. Furthermore, various experimental investigations, including additive studies, kinetic isotope effect measurements, and Eyring analysis were carried out to probe the reaction kinetics and mechanism of the Csp^3–H bond activation by the Pd(II) center. A combined experimental and theoretical mechanistic analysis suggests that acetate-assisted Csp^3–H bond activation is preferred at high temperature, while acetate-free is preferred at room temperature. These results provide insights into the important process of Csp^3–H bond activation by Pd complexes that seems to be operative under mild conditions and without a base additive, and thus could be employed in a wider range of C-H functionalization reactions.

Results and discussion

Ligand synthesis. Our group has previously utilized the macrocyclic *N,N*'-dialkyl-2,11-diaza[3.3](2,6)pyridinophane (^{R}N4) ligands to study a variety of transition metal complexes.[8-20] As a continuation of our studies, we sought to further extend the denticity of the pyridinophane ligand framework through the attachment of a coordinating 2-methylpyridyl arm (2-picolyl, Pic), which results in a new type of pentadentate ligand, *N*-methyl-N'-(2-methylpyryl)-2,11-diaza[3.3](2,6)pyridinophane (^{PicCH3}N4, Scheme 1). The synthesis of ^{PicCH3}N4 started with the previously reported unsymmetric pyridinophane precursor, *N*-tosyl-2,11-diaza[3.3](2,6)pyridinophane (^{TsH}N4).[31] Addition of 2-(chloromethyl)-pyridine hydrochloride into ^{TsH}N4 with diisopropylethylamine in the presence of a catalytic amount of tetrabutylammonium bromide (TBABr) generated ^{TsPic}N4 in 89% yield. The detosylation and subsequent methylation through the Eschweiler-Clarke reaction afforded the desired ligand ^{PicCH3}N4 in 60% overall yield. In addition, the deuterated variant ^{PicCD3}N4, which was employed in mechanistic studies (see below), was synthesized through the Eschweiler-Clarke reaction of

^{PicH}N4 with 20% formaldehyde-d_2 in D_2O and formic acid-d_2. ^{1}H NMR spectroscopic analysis of the obtained ^{PicCD3}N4 ligand confirmed the absence of CH_3 functional group, while the ^{2}H NMR spectrum clearly indicates the presence of CD_3 group (Figure S4).

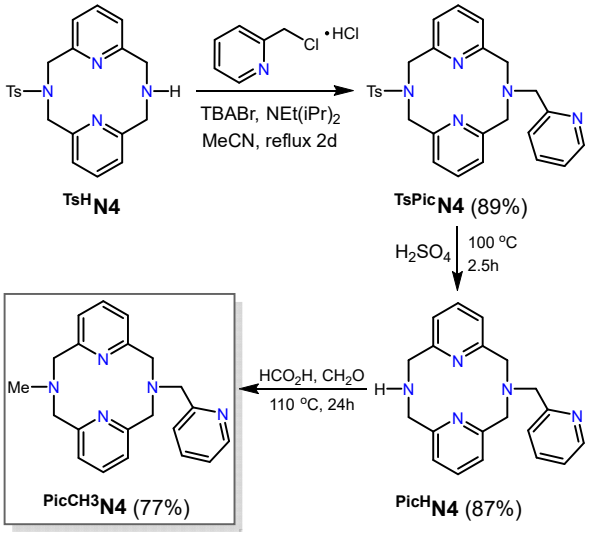

Scheme 1. Synthesis of newly developed ligand ^{PicCH3}N4.

Synthesis and characterization of Pd complexes. With the newly developed ligand in hand, the synthesis of the corresponding Pd^{II} complex was attempted through the reaction of ^{PicCH3}N4 with $[Pd^{II}(MeCN)_4](BF_4)_2$ in MeCN at room temperature. Interestingly, the product obtained from the reaction of ^{PicCH3}N4 with $[Pd^{II}(MeCN)_4]^{2+}$ was found to be an unexpected Pd complex, $[(^{PicCH2}N4)Pd^{II}]^+$ (**1**), according to the single-crystal X-ray crystallography (Scheme 2) and ^{1}H NMR spectroscopic analysis (Figures S5–S9). Rather than the coordination of N-donor atom in N–CH_3 arm, C–H activation of the methyl group by Pd resulted in the formation of palladacycle **1**. Notably, the C–H activation occurs at room temperature, affording **1** in 34% yield, although the reaction requires 60 h. Warming up the reaction temperature to 50 °C marginally increased the yield of **1**, and heating at temperatures higher than 70 °C resulted in

decomposition. Instead, **1** can be obtained in a higher yield of 82% in the presence of NaOAc and upon heating at 60 °C with significantly reduced reaction time (3 h, Scheme 2). Complex **1** is a diamagnetic Pd^{II} species d^8 that was characterized by ^1H NMR spectroscopy. The evidence for C–H activation was supported by the absence of a chemical resonance corresponding to methyl protons (N-CH_3 at 2–3 ppm) and the presence of a downfield singlet corresponding to the methylene protons at 3.97 ppm (Figures S5–S9). X-ray quality crystals for **1** were obtained by slow diffusion of diethyl ether into a concentrated MeCN solution. X-ray crystal structure analysis of **1** reveals a square pyramidal geometry around the Pd^{II} center with the structural parameter $\tau_5 = 0.07$ (Figure 1, left).[32] The Pd–C bond distance of 2.017(2) Å is comparable to the previously reported values of Pd–C bond in palladacycles formed via C–H activation.[33-34] As the reaction of ^{PicCH3}N4 with $[Pd^{II}(MeCN)_4]^{2+}$ in the presence of NaOAc led to the formation of **1** in higher yield, we set out to probe whether a change of Pd precursor to $Pd(OAc)_2$ would readily generate **1**. However, the reaction of ^{PicCH3}N4 and $Pd(OAc)_2$ did not yield **1**, but instead afforded a four-coordinate acetate-bound Pd^{II} complex $[(^{PicCH3}N4)Pd^{II}(OAc)]^+$ (**2**), with one of the pyridine rings and the N–CH_3 donor atom not interacting with the Pd center (Scheme 2 and Figure 1). The C–H activation was not observed upon heating the reaction mixture up to 60 °C. In contrast to **1**, ^1H NMR spectrum of **2** exhibits a methyl peak (N–CH_3) chemical shift at 2.76 ppm, which is similar to those observed for several $(^{Me}N4)Pd^{II}$ complexes, indicating that C–H activation did not occur in this case (Figure S10).[35-36] The structure of **2** reveals a square planar geometry of the Pd^{II} center, bonded to the three N donor atoms (two pyridine N atoms and one of the amine N atoms) of the ligand. The last coordination site is occupied by an acetate ligand, therefore positioning the methyl amine group far away (~4.4 Å) from the Pd metal center. These geometric considerations suggest that C–H activation is prevented due to the acetate binding, thus inhibiting an interaction between the Pd center and the C–H bond.

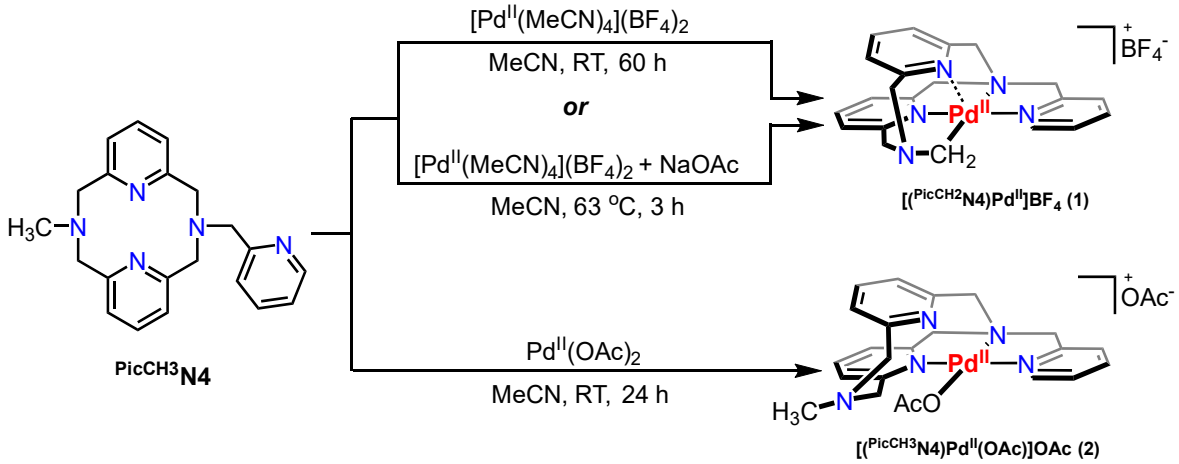

Scheme 2. Synthesis of Pd^{II} complexes.

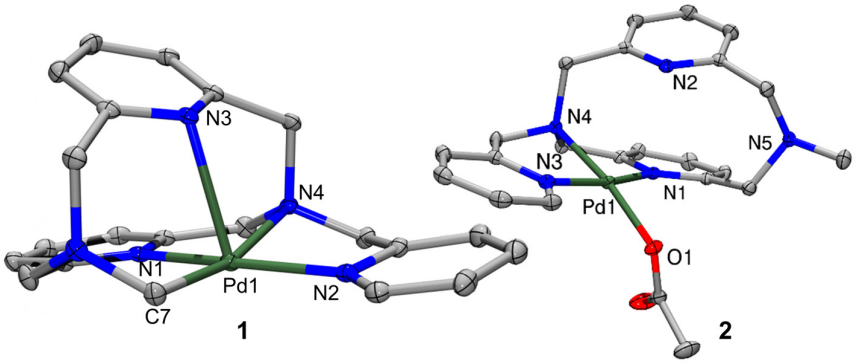

Figure 1. ORTEP representation of the cations of **1** (left) and **2** (right). Ellipsoids are shown at the 50% probability level with hydrogen atoms and counter ions are omitted for clarity. Selected bond distances (Å): **1**, Pd1–C7 2.017(2), Pd1–N1 2.0633(17), Pd1–N2 2.0695(18), Pd1–N3 2.5495(16), Pd1–N4 2.1677(16); **2**, Pd1–O1 2.0191(1), Pd1–N1 2.0432(1), Pd1–N3 1.9940(1), Pd1–N4 2.0220(1).

Electrochemical and Electron Paramagnetic Resonance (EPR) Studies. Due to the intriguing structure and the formation of **1**, its electrochemical properties were investigated by cyclic voltammetry (CV, Figure 2a). The CV of **1** in MeCN reveals an irreversible oxidation wave at 0.72 V vs $Fc^{+/0}$, which is assigned to the $Pd^{III/IV}$ couple. A pseudoreversible wave at –

0.21 V vs $Fc^{+/0}$ likely corresponds to the $Pd^{II/III}$ couple, as observed previously for a related Pd^{II} complex (^{tBu}N4)PdMeCl.[36-37] When ^{PicCH3}N4 and $[Pd^{II}(MeCN)_4]^{2+}$ are mixed and analyzed *in-situ*, a different voltammogram profile was observed, indicating that the C–H activation of the methyl group and the addition of the methylene donor ligand drastically changes the electrochemistry of the Pd^{II} complex (Figure S13). By contrast, the non C-H activated species $[(^{PicCH3})Pd^{II}]^{2+}$ exhibits higher oxidation events at 0.964 V vs $Fc^{+/0}$ and 1.20 V vs $Fc^{+/0}$, as expected for a Pd species with a higher overall charge. As the oxidation potential of **1** is chemically accessible, **1** was oxidized with 1 equiv. ferrocenium tetrafluoroborate ($FcBF_4$) to generate a green species that is tentatively assigned as $[(^{PicCH2})N4Pd^{III}]^{2+}$ (**1**$^+$). The EPR spectrum of **1**$^+$ recorded at 77 K in 1:3 = MeCN:PrCN reveals a pseudoaxial signal with g_x = 2.056 (A_x = 18 G), g_y = 2.083, (A_y = 19 G), and g_z = 2.277 (A_z = 5 G) with superhyperfine coupling to three N atoms in the (Figure 2b). These g values are similar to those typically observed for Pd^{III} d^7 ions such as the ones in (^{tBu}N4)$Pd^{III}(X)_2$ or (^{Me}N4)$Pd^{III}(X)_2$ complexes.[38] However, the ordering of the *g* values ($g_z > g_x, g_y$) is different from that of most reported EPR spectra of six-coordinated mononuclear Pd^{III} complexes in a distorted octahedral geometry with a $(d_{z2})^1$ ground state.[39] This ordering of the *g* values is consistent with the Pd^{III} center with five-coordinate square pyramidal geometry and a $(d_{xy})^1$ or $(d_{x2-y2})^1$ ground state, as observed previously.[40] In addition, a splitting pattern due to the superhyperfine coupling to three N atoms with the Pd center is observed in both x and y directions, which is in line with a five-coordinate square pyramidal geometry. A similar splitting pattern in the x and y directions has been observed in the $[(N2S2)Pd^{III}MeCl]^+$ complex, which was suggested to have five-coordinate geometry with N atoms in the equatorial plane.[40]

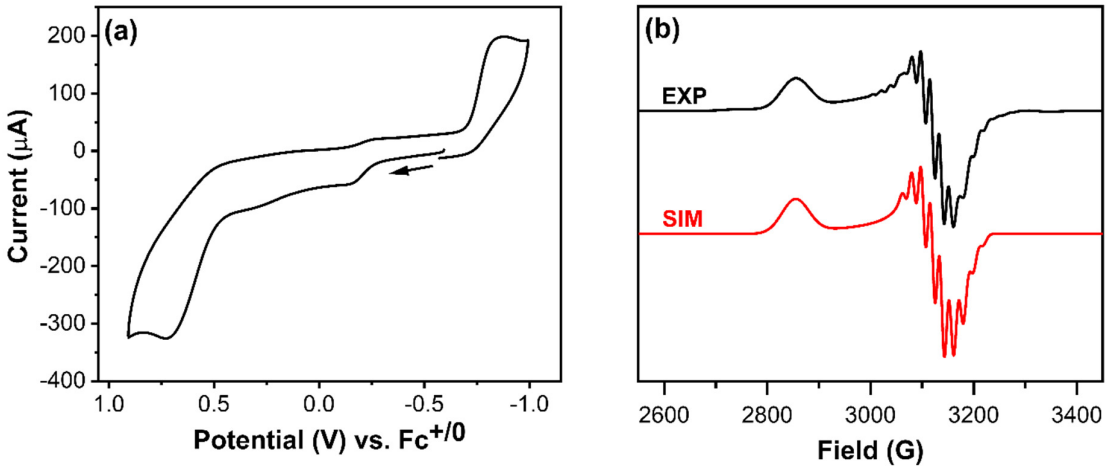

Figure 2. (a) Cyclic voltammogram (CV) of **1** in 0.1 M Bu_4NClO_4/MeCN (scan rate 0.1 V/s). (b) EPR spectrum (black line) of **1** after treating with 1 equiv. of $FcBF_4$ in 1:3 MeCN:PrCN glass at 77 K. The following g values were used for the simulation (red line): $g_x = 2.056$ (A_x = 18 G), $g_y = 2.083$, (A_y = 19 G), and $g_z = 2.277$ (A_z = 5 G).

Effect of additives and reaction conditions for C–H activation. The observed Csp^3–H activation of the ligand and formation of **1** prompted us to investigate its kinetics and reaction mechanism. First, since it is commonly know that a base additive is cam promote the C–H activation step via a concerted metalation-deprotonation (CMD) process, we have investigated the effect of various base additives on the formation of **1** (Table 1). The addition of 1,8-bis(dimethylamino)naphthalene (proton sponge), lithium hexamethyldisilazide (LiHMDS), or tetramethylammonium mesylamide (NMe_4MsNH) failed to induce the activation of C–H bond by the Pd^{II} center, and Pd complex decomposition occurred instead . Although no intermediate was identified in our case, the proton sponge and Pd precursor might form a transient complex, since the crystal structure of a proton sponge-Pd complex was reported previously.[41-43] Both LiHMDS and NMe_4MsNH are strong bases that can deprotonate the benzylic positions of the pyridinophane ligand, it is expected that such strong based would generate unidentified Pd complex or ledd to decomposition. By contrast, the addition of NaOAc to the reaction mixture at room temperature was found to slightly increase the yield of **1** up to 43%. Increasing the reaction temperature to 63°C led to the considerable enhancement of the yield up to 82% within

3 h, and we posited this temperature effect might arise from the solubility enhancement of NaOAc. As this condition yielded a fast and clean formation of **1**, the kinetic isotope effects (KIE) measurements were performed with NaOAc as additive at 63°C, as discussed in the next section. As the addition of NaOAc leads to appreciable product formation, other carboxylates such as cesium pivalate (CsOPiv), silver acetate (AgOAc), and tetrabutylammonium acetate (TBAOAc) were also tested. Surprisingly, these carboxylate additives did not lead to any C–H activation at room temperature. When heated, the signature ^{1}H NMR peaks for **1** were observed, but the yield was less than 10% and a variety of other unidentified peaks were observed, indicating the formation of other Pd species or decomposition. Considering the higher solubility of CsOPiv, AgOAc, and TBAOAc compared to that of NaOAc, we suspect that stable acetate-coordinated Pd species are preferably formed with these soluble acette salts and this leads to inhibition of C–H activation, as seen in the case when $Pd(OAc)_2$ was used as the precursor (Scheme 2 and Figure 1). Given these observations, a substoichiometric amount of TBAOAc salt was employed to see if this would increase the formation of **1**. Indeed, addition of only 0.5 equiv TBAOAc generates 80% of **1** in 5 h, while addition of 0.33 equiv TBAOAc led to a faster conversion, achieving 80% yield of **1** in 1 h (Table 1). This trend further supports our hypothesis that a stoichiometric amount of acetate present in solution inhibits C–H activation due to the competing acetate binding to the Pd metal center, generating a coordinatively saturated species in which no weak interaction between the C–H and the Pd is possible. In addition, the formation of **1** in the presence of acetate seems to require the dissociation of acetate from the Pd complex – which can be achieved at higher temperatures, in order to allow a weak interaction between the Pd metal center and the C–H bond that precedes C–H activation. Overall, all these results from the experiments with various equiv of additives imply that the low solubility of the NaOAc or substoichiometric amounts of soluble TBAOAc are crucial for limiting the formation of coordinatively saturated Pd-acetate species

and thus lead to efficient C–H bond activation.

Table 1. Conditions for C–H Activation of ^{PicCH3}N4 ligand with various additives

Additive	Equiv	Temp (°C)	Time (h)	Yield of 1 (%)
None	NA	25	60	34%
	NA	50	24	39%
	NA	70	24	0%[b]
NaOAc	2	25	73	43%
	2	63	3	82%
Proton sponge	1	25	24	0%[a]
LiHMDS	1	25	0.5	0%[b]
NMe_4MsNH	1	25	0.5	0%[b]
CsOPiv	1	25	60	0%[a]
	1	63	24	6%
AgOAc	1	25	60	0%[a]
	1	63	24	7%
TBAOAc	1	63	48	0%[a]
	0.5	63	5	80%
	0.33	63	1	80%
	0.25	63	0.5	48%
	0.1	63	0.5	43%

[a] Unidentified Pd products observed other than starting material or **1**, [b] Decomposition of unidentified Pd product observed other than starting material or **1**. NA – not applicable.

Reaction kinetics and thermodynamics. To gain insight into the C–H activation process, kinetic isotope effects (KIE) measurements were performed. The growth of the methylene peak (Pd–CH_2) from the reaction of $[Pd(MeCN)_4]^{2+}$ with ^{PicCH3}N4 or ^{PicCD3}N4 ligand in the presence of NaOAc in CD_3CN at 63°C was monitored using ^{1}H and ^{2}H NMR, respectively (Figures S14 and S15). The conversion into **1** was best fit to a double exponential decay, following equation (1).

$$y = y_0 + A_1 e^{k_1 x} + A_2 e^{k_2 x} \quad (1)$$

Two rate constants k_1 and k_2 were determined to be $k_1 = 5.2(8)$ h^{-1} and $k_2 = 0.92(4)$ h^{-1} for the growth of the Pd–CH_2 methylene peak when ^{PicCH3}N4 was used as the ligand. With ^{PicCD3}N4,

the rate constants k_1 = 2.66(7) h^{-1} and k_2 = 0.084(1) h^{-1} were obtained, respectively. These two parallel reactions result in observed KIEs of k_H/k_D = 1.95 and 11.0 for the fast and slow first-order decays, respectively, and are thus tentatively assigned to a pre-equilibrium formation of a Pd···H–C interaction, followed by the slower and rate-determining C–H bond cleavage step.[44-46] To obtain further insight, we have performed an Eyring analysis by measuring the rates of the formation of **1** at three different reaction temperatures (43 °C, 53 °C, and 63 °C), with and without the NaOAc additive present. Analysis of the temperature dependence of the rate constants by plotting ln(k/T) vs 1/T resulted in a straight line that gave the activation parameters $\Delta H^{\ddagger}$ = 10.0 ± 1 kcal/mol and $\Delta S^{\ddagger}$ = –42.0 ± 3 kcal/mol·K in the absence of NaOAc, and $\Delta H^{\ddagger}$ = 31.0 ± 1 kcal/mol and $\Delta S^{\ddagger}$ = 24.0 ± 2 kcal/mol·K in the presence of NaOAc (Figure 3). Without NaOAc, a large negative entropy of activation ($\Delta S^{\ddagger}$) was obtained, indicating the formation of an ordered transition state, likely due to a bimolecular reaction. This correlates well with the DFT-calculated transition state that involves a deprotonation step assisted by the pyridyl group of another ^{PicCH3}N4 ligand (see below, Figure 4). On the other hand, in the presence of NaOAc additive a positive value of $\Delta S^{\ddagger}$ is obtained, indicating that either dissociation of acetate from Pd complex is required prior to C–H activation, or an acetate-bound Pd species is involved in the transition state and deprotonation is performed by the pre-coordinated acetate, akin to a typical CMD mechamism. Interestingyly, at room temperature a Gibbs activation energy of $\Delta G^{\ddagger}$ = 22 kcal/mol was obtained in the reaction without NaOAc, which is slightly smaller than that obtained in the presence of NaOAc ($\Delta G^{\ddagger}$ = 24 kcal/mol). However, at a higher temperature the opposite trend was observed: the calculated value of $\Delta G^{\ddagger}$ = 23 kcal/mol in the reaction with NaOAc at 63 °C is lower than that of the reaction without NaOAc ($\Delta G^{\ddagger}$ = 24 kcal/mol). These results are in line with the increased yield of **1** obtained in a shorter time with NaOAc at elevated temperatures, as observed experimentally (Table 1), and support the general conditions employed in Pd-mediated C-H bond activation that employ

acetate additives and elevated temperatures. In addition, these results also reveal an important finding that acetate-free C–H bond activation by Pd centers can actually occur at room temperatures, and it may even be preferred to acetate-mediated C-H bond activation, although presence of base seems to be needed for neutralizing the generated protons and increase the C–H activated product yield.

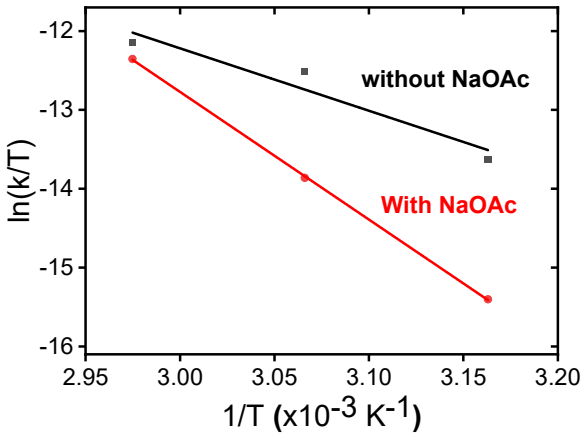

	without NaOAc	with NaOAc
$\Delta H^{\ddagger}$ ($\frac{kcal}{mol}$)	10.0 ± 1	31.0 ± 1
$\Delta S^{\ddagger}$ ($\frac{kcal}{mol\ K}$)	**-42.0 ± 3**	**24.0 ± 2**
$\Delta G^{\ddagger}$ (298 K, $\frac{kcal}{mol}$)	**22.0 ± 1**	24.0 ± 1
$\Delta G^{\ddagger}$ (336 K, $\frac{kcal}{mol}$)	24.0 ± 1	**23.0 ± 1**

Figure 3. Eyring plot for the generation of **1** obtained from the growth of methylene peak (Pd–CH_2) and activation parameters obtained from Eyring analysis.

DFT calculations. With these experimental results in hand, we then performed density functional theory (DFT) calculations to provide support for the proposed reaction mechanism. All calculations were performed by employing the B3LYP-D3/LACVP/6-31G** level of theory for the geometry optimization, vibrational analysis, and solvation energy calculations. The electronic energies of all optimized structures were reevaluated with B3LYP-D3/LACV3P/cc-pVTZ(-f).[40-50] Further computational details are given in the Supporting

information. The energy profile of the proposed reaction mechanism in the absence of acetate additive is shown in Figure 4.

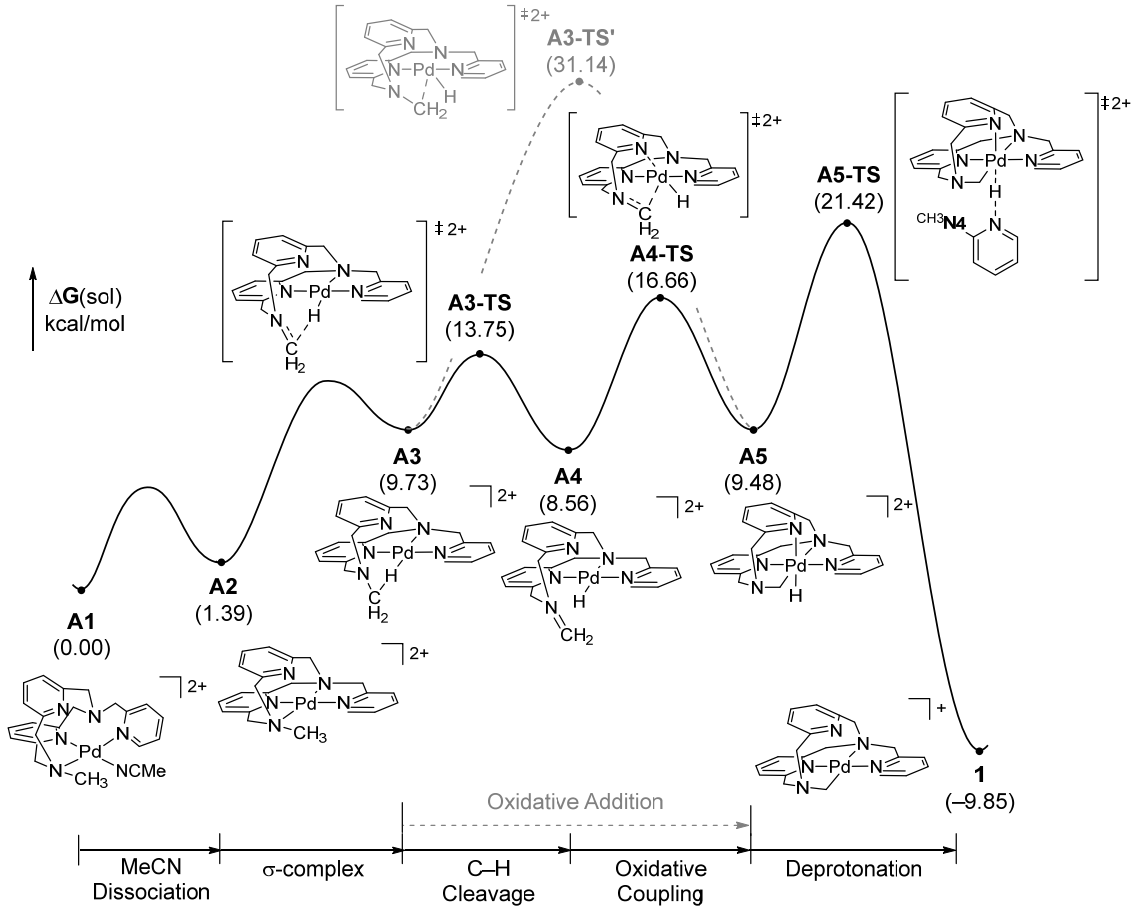

Figure 4. DFT-calculated energy profile for the Pd-mediated C–H activation of ^{PicCH3}N4, describing the reaction mechanism of generating **1** in the absence of acetate additive.

The reaction initiates with the formation of σ-complex (**A3**), which is located at 9.7 kcal/mol higher energy than the unactivated (^{PicCH3}N4)Pd species. Next, the Csp^3–H bond of **A3** is cleaved through the **A3-TS** transition state that has a barrier of 13.8 kcal/mol, which involves a hydride abstraction to generate a Pd-hydride species and a methyleneiminium intermediate **A4**. The methyleneiminium carbocation then undergoes oxidative addition to the Pd center, leading to the formation of a Pd(IV) species **A5** at 9.5 kcal/mol via a transition state **A4-TS** with a barrier of 16.7 kcal/mol. This step-wise C–H activation process is expected to be more

facile than the concerted mechanism, which involves C–H cleavage through oxidative addition *via* **A3-TS'**, with a barrier of 31.1 kcal/mol.[47-52] Finally, **A5** is reduced through deprotonation by the pyridyl group of another ^{PicCH3}N4 ligand *via* **A5-TS** that has the highest barrier of the overall reaction at 21.4 kcal/mol, to ultimately generate observed product **1** at –9.9 kcal/mol. Importantly, since a second equivalent of ^{PicCH3}N4 is acting as base to remove the proton formed upon C–H cleavage, the yield of **1** is expected to be lower than 50%, which is consistent with the experimental result (Table 1).

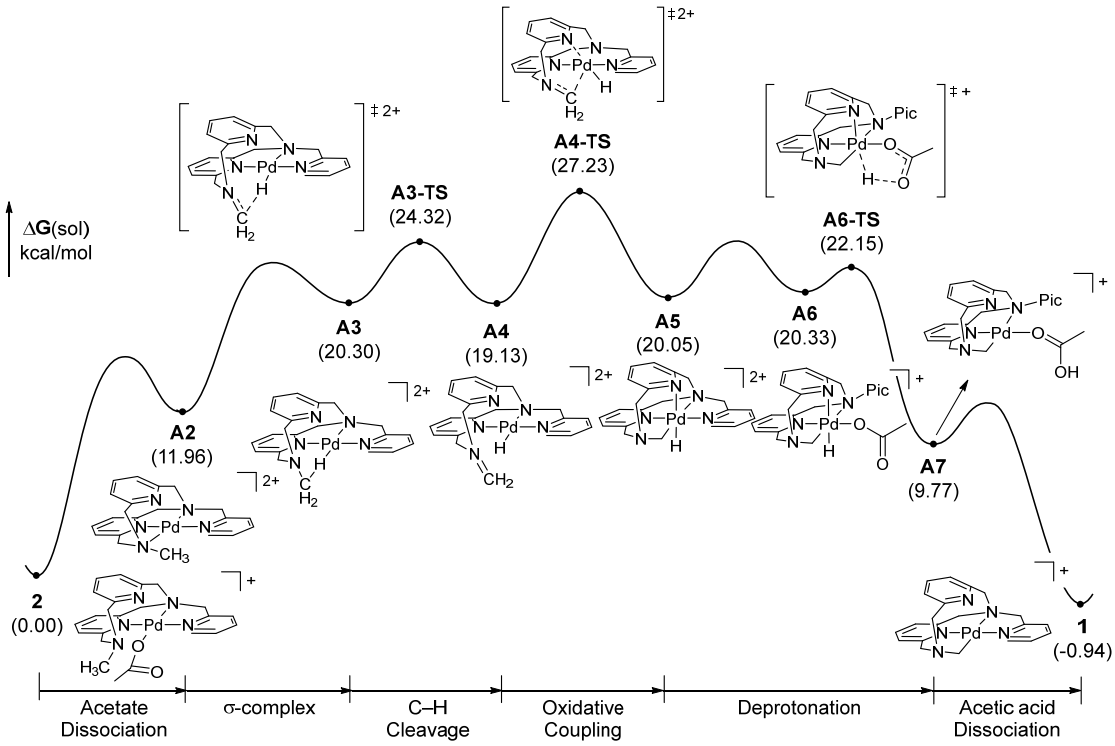

Figure 5. DFT-calculated energy profile for the Pd-mediated C–H activation of ^{PicCH3}N4, describing the reaction mechanism of generating **1** in the presence of acetate additive.

Figure 5 summarizes the results of examining the mechanism for the formation of **1** in the presence of acetate. The calculations suggest that the Pd-acetate complex **2** is the resting state of the reaction in the presence of acetate. Complex **2** is 10.6 kcal/mol more stable than **A1**, the resting state of the reaction without acetate, resulting in an increased overall barrier for

the oxidative addition of 27.2 kcal/mol, despite the C–H activation mechanism being identical to that proposed for the reaction without acetate present (Figure 4). These results indicate that the reaction in the presence of acetate may require a higher reaction temperature (Table 1). An alternate mechanism was also considered, that is the conventional concerted metalation-deprotonation (CMD) process in which the Pd-bound acetate promotes the C–H activation.[51-56] However, the calculations suggest the CMD process is not feasible as it has an insurmountable barrier of 37.1 kcal/mol, and likely due to the repulsion between the lone pair of the axial pyridine N atom and the dz^2 orbital of the Pd center (Figure S21). After oxidative addition to generate the Pd(IV) intermediate **A5**, acetate binding would generate **A6**, followed by acetate-assisted deprotonation *via* the **A6-TS** transition state at 22.2 kcal/mol. Finally, the dissociation of acetic acid at **A7** leads to the desired product **1**. Overall, the proposed mechanism implies that in the presence of acetate the yield is not limited to < 50%, in line with the experimental results that show an improved yield of **1** at higher temperatures in the presence of acetate (Table 1).

Conclusion

In conclusion, herein we report a new pentadentate pyridinophane ligand ^{PicCH3}N4 and its Pd^{II} complexes. The reaction of Pd precursor $[Pd^{II}(MeCN)_4]^{2+}$ with ^{PicCH3}N4 gave $[(^{PicCH2}N4)Pd^{II}]^{+}$ (**1**), which formed from the uncommon Csp^3–H activation by Pd^{II} occurring at room temperature. Complex **1** was isolated and characterized by single-crystal X-ray crystallography, NMR, cyclic voltammetry, as well as the EPR characterization of the related one-electron oxidized Pd^{III} speices. In addition, various experimental investigations such as additive studies, KIE measurements, and Eyring analysis were conducted to understand the reaction kinetics and mechanism of the Csp^3–H bond activation by Pd^{II} center. Through a detailed mechanistic analysis, we show that acetate-assisted C–H bond activation is preferred at higher temperatures, while acetate-free C–H activation is preferred at room temperature, which was also supported

by DFT calculations. This could have far reaching implications for transition metal-mediated C–H bond activation processes, showing that such transformations can occur without addition of a base additive, and also that such processes can occur under milder conditions than initially anticipated. Overall, the newly developed macrocyclic pentadentate pyridinophane framework presented herein provides further impetus to explore its applications in coordination chemistry, form organometallic catalysis to bioinorganic chemistry.

Corresponding Authors

Liviu M. Mirica – Department of Chemistry, University of Illinois at Urbana-Champaign, 600 S. Mathews Avenue, Urbana, IL, 61801, USA

Email: mirica@illinois.edu

Mu-Hyun Baik – Center for Catalytic Hydrocarbon Functionalizations, Institute for Basic Science (IBS), Daejeon 34141, Republic of Korea; Department of Chemistry, Korea Advanced Institute of Science and Technology (KAIST), Daejeon 34141, Republic of Korea

Email: mbaik2805@kaist.ac.kr

Authors

Hanah Na – Department of Chemistry, University of Illinois-Urbana Champaign, 600 S. Mathews Avenue, Urbana, IL, 61801, USA

Andrew J. Wessel – Department of Chemistry, Washington University, St. Louis, Missouri, 63130, USA

SeoungTae Kim – Department of Chemistry, Korea Advanced Institute of Science and Technology (KAIST), Daejeon 34141, Republic of Korea; Center for Catalytic Hydrocarbon Functionalizations, Institute for Basic Science (IBS), Daejeon 34141, Republic of Korea

ORCID

Liviu M. Mirica: 0000-0003-0584-9508

Hanah Na: 0000-0002-0576-4806

SeoungTae Kim: 0000-0003-4067-9567

Mu-Hyun Baik: 0000-0002-8832-8187

Acknowledgments

This work was supported by the National Science Foundation (CHE-2102544 to L.M.M.) and the Institute for Basic Science in Korea (IBS-R010-A1 to M.-H.B.). We thank Drs. Brian Marsden, Jeff Kao, and Manmilan Singh for all of their assistance with the array and deuterium NMR techniques.

References

1. G. Melson, *Coordination chemistry of macrocyclic compounds*, Springer Science & Business Media, 2012.
2. S. J. Archibald, *Annu. Rep. Prog. Chem., Sect. A: Inorg. Chem.*, 2009, **105**, 297-322.
3. A. Haque, R. Ilmi, I. J. Al-Busaidi and M. S. Khan, *Coord. Chem. Rev.*, 2017, **350**, 320-339.
4. R. E. Mewis and S. J. Archibald, *Coord. Chem. Rev.*, 2010, **254**, 1686-1712.
5. T. Joshi, B. Graham and L. Spiccia, *Acc. Chem. Res.*, 2015, **48**, 2366-2379.
6. L. Fabbrizzi, *Comments Inorg. Chem.*, 1985, **4**, 33-54.
7. M. Jagoda, S. Warzeska, H. Pritzkow, H. Wadepohl, P. Imhof, J. C. Smith and R. Krämer, *J. Am. Chem. Soc.*, 2005, **127**, 15061-15070.
8. W. O. Koch and H.-J. Krüger, *Angew. Chem., Int. Ed.*, 1995, **34**, 2671-2674.
9. W. O. Koch, A. Barbieri, M. Grodzicki, V. Schünemann, A. X. Trautwein and H.-J. Krüger, *Angew. Chem., Int. Ed.*, 1996, **35**, 422-424.
10. M. Graf, G. Wolmershäuser, H. Kelm, S. Demeschko, F. Meyer and H.-J. Krüger, *Angew. Chem., Int. Ed.*, 2010, **49**, 950-953.
11. J. R. Khusnutdinova, N. P. Rath and L. M. Mirica, *J. Am. Chem. Soc.*, 2010, **132**, 7303-

7305.

12. T. W.-S. Chow, E. L.-M. Wong, Z. Guo, Y. Liu, J.-S. Huang and C.-M. Che, *J. Am. Chem. Soc.*, 2010, **132**, 13229-13239.
13. J. R. Khusnutdinova, N. P. Rath and L. M. Mirica, *J. Am. Chem. Soc.*, 2012, **134**, 2414-2422.
14. F. Z. Tang, Y. Zhang, N. P. Rath and L. M. Mirica, *Organometallics*, 2012, **31**, 6690-6696.
15. J. R. Khusnutdinova, J. Luo, N. P. Rath and L. M. Mirica, *Inorg. Chem.*, 2013, **52**, 3920-3932.
16. B. Zheng, F. Z. Tang, J. Luo, J. W. Schultz, N. P. Rath and L. M. Mirica, *J. Am. Chem. Soc.*, 2014, **136**, 6499-6504.
17. F. Z. Tang, N. P. Rath and L. M. Mirica, *Chem. Comm.*, 2015, **51**, 3113-3116.
18. F. S. Menges, S. M. Craig, N. Tötsch, A. Bloomfield, S. Ghosh, H.-J. Krüger and M. A. Johnson, *Angew. Chem., Int. Ed.*, 2016, **55**, 1282-1285.
19. J. W. Schultz, K. Fuchigami, B. Zheng, N. P. Rath and L. M. Mirica, *J. Am. Chem. Soc.*, 2016, **138**, 12928–12934.
20. J. Serrano-Plana, A. Aguinaco, R. Belda, E. García-España, M. G. Basallote, A. Company and M. Costas, *Angew. Chem., Int. Ed.*, 2016, **55**, 6310-6314.
21. D. Jeong, T. Ohta and J. Cho, *J. Am. Chem. Soc.*, 2018, **140**, 16037-16041.
22. K. Kim, D. Cho, H. Noh, T. Ohta, M.-H. Baik and J. Cho, *J. Am. Chem. Soc.*, 2021, **143**, 11382-11392.
23. H. Sugimoto, K. Ashikari and S. Itoh, *Inorg. Chem.*, 2013, **52**, 543-545.
24. W.-T. Lee, S. B. Muñoz Iii, D. A. Dickie and J. M. Smith, *Angew. Chem., Int. Ed.*, 2014, **53**, 9856-9859.
25. W.-P. To, T. Wai-Shan Chow, C.-W. Tse, X. Guan, J.-S. Huang and C.-M. Che, *Chem. Sci.*, 2015, **6**, 5891-5903.
26. A. Roca-Sabio, C. S. Bonnet, M. Mato-Iglesias, D. Esteban-Gómez, É. Tóth, A. d. Blas, T. Rodríguez-Blas and C. Platas-Iglesias, *Inorg. Chem.*, 2012, **51**, 10893-10903.
27. G. Castro, R. Bastida, A. Macías, P. Pérez-Lourido, C. Platas-Iglesias and L. Valencia, *Inorg. Chem.*, 2013, **52**, 6062-6072.
28. N. Bandara, A. K. Sharma, S. Krieger, J. W. Schultz, B. H. Han, B. E. Rogers and L. M. Mirica, *J. Am. Chem. Soc.*, 2017, **139**, 12550-12558.
29. A. K. Sharma, J. W. Schultz, J. T. Prior, N. P. Rath and L. M. Mirica, *Inorg. Chem.*, 2017, **56**, 13801-13814.
30. Y. Huang, T. T. Huynh, L. Sun, C.-H. Hu, Y.-C. Wang, B. E. Rogers and L. M. Mirica,

Inorg. Chem., 2022, **61**, 4778–4787.

31. A. J. Wessel, J. W. Schultz, F. Tang, H. Duan and L. M. Mirica, *Org. Biomol. Chem.*, 2017, **15**, 9923-9931.
32. A. W. Addison, T. N. Rao, J. Reedijk, J. van Rijn and G. C. Verschoor, *J. Chem. Soc., Dalton Trans.*, 1984, 1349-1356.
33. P. Halder, D. J. SantaLucia, S. V. Park and J. F. Berry, *Inorg. Chem.*, 2019, **58**, 2270-2274.
34. W. H. Henderson, J. M. Alvarez, C. C. Eichman and J. P. Stambuli, *Organometallics*, 2011, **30**, 5038-5044.
35. F. Tang, Y. Zhang, N. P. Rath and L. M. Mirica, *Organometallics*, 2012, **31**, 6690-6696.
36. F. Tang, F. Qu, J. R. Khusnutdinova, N. P. Rath and L. M. Mirica, *Dalton Trans.*, 2012, **41**, 14046-14050.
37. J. R. Khusnutdinova, N. P. Rath and L. M. Mirica, *Inorg. Chem.*, 2014, **53**, 13112-13129.
38. F. Z. Tang, S. V. Park, N. P. Rath and L. M. Mirica, *Dalton Trans.*, 2018, **47**, 1151-1158.
39. J. R. Khusnutdinova and L. M. Mirica, in *C-H and C-X Bond Functionalization: Transition Metal Mediation*, ed. X. Ribas, Royal Society of Chemistry, 2013, ch. 5, pp. 122-158.
40. J. Luo, N. P. Rath and L. M. Mirica, *Organometallics*, 2013, **31**, 3343-3353.
41. G. Villaverde, A. Arnanz, M. Iglesias, A. Monge, F. Sanchez and N. Snejko, *Dalton Trans.*, 2011, **40**, 9589-9600.
42. Y. Tomoki, O. Nobutaka, S. Yasunari, O. Kozo, G. Kenji, N. Fumiko, H. Masato and O. Seichi, *Chem. Lett.*, 2004, **33**, 928-929.
43. U. Wild, O. Hübner, A. Maronna, M. Enders, E. Kaifer, H. Wadepohl and H.-J. Himmel, *Eur. J. Inorg. Chem.*, 2008, **2008**, 4440-4447.
44. E. M. Simmons and J. F. Hartwig, *Angew. Chem., Int. Ed.*, 2012, **51**, 3066-3072.
45. T. W. Lyons and M. S. Sanford, *Chem. Rev.*, 2010, **110**, 1147-1169.
46. M. Gomez-Gallego and M. A. Sierra, *Chem. Rev.*, 2011, **111**, 4857-4963.
47. D. Balcells, E. Clot and O. Eisenstein, *Chem. Rev.*, 2010, **110**, 749-823.
48. L. Ackermann, *Chem. Rev.*, 2011, **111**, 1315-1345.
49. J. He, M. Wasa, K. S. L. Chan, Q. Shao and J.-Q. Yu, *Chem. Rev.*, 2017, **117**, 8754-8786.
50. M. Lafrance and K. Fagnou, *J. Am. Chem. Soc.*, 2006, **128**, 16496-16497.
51. Á. Gutiérrez-Bonet, F. Juliá-Hernández, B. de Luis and R. Martin, *J. Am. Chem. Soc.*, 2016, **138**, 6384-6387.
52. D. Lapointe and K. Fagnou, *Chem. Lett.*, 2010, **39**, 1118-1126.

TOC Graphical abstract

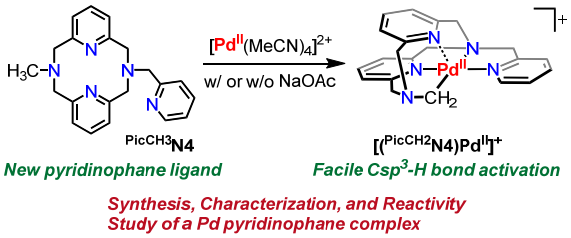

A pentadentate pyridinophane ligand is reported, along with a palladacycle product generated via Csp^3–H bond activation under mild conditions.